AFRL-OSR-VA-TR-2015-0136

Physical and Chemical Processes in Turbulent Flames

Chung Law
TRUSTEES OF PRINCETON UNIVERSITY

06/23/2015
Final Report

Air Force Research Laboratory
AF Office Of Scientific Research (AFOSR)/ RTE
Arlington, Virginia 22203
Air Force Materiel Command

Report Documentation Page

Form Approved
OMB No. 0704-0188

1. REPORT DATE	2. REPORT TYPE	3. DATES COVERED
23 JUN 2015		**15-03-2013 to 14-03-2015**

4. TITLE AND SUBTITLE	5a. CONTRACT NUMBER
Physical and Chemical Processes in Turbulent Flames	5b. GRANT NUMBER
	5c. PROGRAM ELEMENT NUMBER
6. AUTHOR(S)	5d. PROJECT NUMBER
	5e. TASK NUMBER
	5f. WORK UNIT NUMBER
7. PERFORMING ORGANIZATION NAME(S) AND ADDRESS(ES) **Princeton University,,Dept. MAE,40 Olden Street,,Princeton,,NJ,08544**	8. PERFORMING ORGANIZATION REPORT NUMBER
9. SPONSORING/MONITORING AGENCY NAME(S) AND ADDRESS(ES)	10. SPONSOR/MONITOR'S ACRONYM(S)
	11. SPONSOR/MONITOR'S REPORT NUMBER(S)

12. DISTRIBUTION/AVAILABILITY STATEMENT
Approved for public release; distribution unlimited

13. SUPPLEMENTARY NOTES

14. ABSTRACT

The two-year subject program, conducted through tight coupling between experiment, theory and computation, and reported in high impact journal articles, has focused on the dynamics of turbulent flames mainly for hydrocarbon fuels in environments simulating various operational aspects of aero-engines. The thrust for this program constitutes of three major areas of turbulent combustion: (1) Flame surface statistics, (2) Flame-turbulence interaction, and (3) Effects of turbulence on the growth of ignition kernel. The research conducted through this program revealed a self similar evolution of flame surface geometry under the influence of turbulent eddies at different turbulence intensities. Moreover, the flame-turbulence interactions were quantified by comparing the evolutions of stretch rates on the flame surface due to flow strain and curvature as the flame grows. Finally, the role of turbulence on ignition was studied to show that for certain condition, turbulence can promote the growth of ignition kernel and thus success of the ignition process.

15. SUBJECT TERMS

16. SECURITY CLASSIFICATION OF:			17. LIMITATION OF ABSTRACT	18. NUMBER OF PAGES	19a. NAME OF RESPONSIBLE PERSON
a. REPORT	b. ABSTRACT	c. THIS PAGE			
unclassified	**unclassified**	**unclassified**	**Same as Report (SAR)**	**34**	

REPORT DOCUMENTATION PAGE

Form Approved
OMB No. 0704-0188

PLEASE DO NOT RETURN YOUR FORM TO THE ABOVE ORGANIZATION.

1. REPORT DATE *(DD-MM-YYYY)*	2. REPORT TYPE	3. DATES COVERED *(From - To)*
12-06-2015	Final Report	3-15-2013 - 3-14-2015

4. TITLE AND SUBTITLE
PHYSICAL AND CHEMICAL PROCESSES IN TURBULENT FLAMES

5a. CONTRACT NUMBER
FA9550-13-1-0119

5b. GRANT NUMBER
FA9550-13-1-0119

5c. PROGRAM ELEMENT NUMBER

6. AUTHOR(S)
Law, Chung, K,
Wu, Fujia,
Saha, Abhishek,
Chaudhuri, Swetaprovo,

5d. PROJECT NUMBER

5e. TASK NUMBER

5f. WORK UNIT NUMBER

7. PERFORMING ORGANIZATION NAME(S) AND ADDRESS(ES)
Princeton University
Dept. MAE
40 Olden Street
Princeton, NJ-08544, USA

8. PERFORMING ORGANIZATION REPORT NUMBER

9. SPONSORING/MONITORING AGENCY NAME(S) AND ADDRESS(ES)
Air Force Office of Scientific Research

10. SPONSOR/MONITOR'S ACRONYM(S)
AFOSR

11. SPONSOR/MONITOR'S REPORT NUMBER(S)

12. DISTRIBUTION/AVAILABILITY STATEMENT
Publicly Available

13. SUPPLEMENTARY NOTES

14. ABSTRACT

The two-year subject program, conducted through tight coupling between experiment, theory and computation, and reported in high impact journal articles, has focused on the dynamics of turbulent flames mainly for hydrocarbon fuels in environments simulating various operational aspects of aero-engines. The thrust for this program constitutes of three major areas of turbulent combustion: (1) Flame surface statistics, (2) Flame-turbulence interaction, and (3) Effects of turbulence on the growth of ignition kernel. The research conducted through this program revealed a self similar evolution of flame surface geometry under the influence of turbulent eddies at different turbulence intensities. Moreover, the flame-turbulence interactions were quantified by comparing the evolutions of stretch rates on the flame surface due to flow strain and curvature as the flame grows. Finally, the role of turbulence on ignition was studied to show that for certain condition, turbulence can promote the growth of ignition kernel and thus success of the ignition process.

15. SUBJECT TERMS
Turbulent Flames, Ignition, High Speed PIV, Strech rates

16. SECURITY CLASSIFICATION OF:			17. LIMITATION OF ABSTRACT	18. NUMBER OF PAGES	19a. NAME OF RESPONSIBLE PERSON
a. REPORT	b. ABSTRACT	c. THIS PAGE			Chung K Law
U	U	U	UU	28	19b. TELEPHONE NUMBER *(Include area code)* 609-258-5271

Reset

INSTRUCTIONS FOR COMPLETING SF 298

1. REPORT DATE. Full publication date, including day, month, if available. Must cite at least the year and be Year 2000 compliant, e.g. 30-06-1998; xx-06-1998; xx-xx-1998.

2. REPORT TYPE. State the type of report, such as final, technical, interim, memorandum, master's thesis, progress, quarterly, research, special, group study, etc.

3. DATES COVERED. Indicate the time during which the work was performed and the report was written, e.g., Jun 1997 - Jun 1998; 1-10 Jun 1996; May - Nov 1998; Nov 1998.

4. TITLE. Enter title and subtitle with volume number and part number, if applicable. On classified documents, enter the title classification in parentheses.

5a. CONTRACT NUMBER. Enter all contract numbers as they appear in the report, e.g. F33615-86-C-5169.

5b. GRANT NUMBER. Enter all grant numbers as they appear in the report, e.g. AFOSR-82-1234.

5c. PROGRAM ELEMENT NUMBER. Enter all program element numbers as they appear in the report, e.g. 61101A.

5d. PROJECT NUMBER. Enter all project numbers as they appear in the report, e.g. 1F665702D1257; ILIR.

5e. TASK NUMBER. Enter all task numbers as they appear in the report, e.g. 05; RF0330201; T4112.

5f. WORK UNIT NUMBER. Enter all work unit numbers as they appear in the report, e.g. 001; AFAPL30480105.

6. AUTHOR(S). Enter name(s) of person(s) responsible for writing the report, performing the research, or credited with the content of the report. The form of entry is the last name, first name, middle initial, and additional qualifiers separated by commas, e.g. Smith, Richard, J, Jr.

7. PERFORMING ORGANIZATION NAME(S) AND ADDRESS(ES). Self-explanatory.

8. PERFORMING ORGANIZATION REPORT NUMBER. Enter all unique alphanumeric report numbers assigned by the performing organization, e.g. BRL-1234; AFWL-TR-85-4017-Vol-21-PT-2.

9. SPONSORING/MONITORING AGENCY NAME(S) AND ADDRESS(ES). Enter the name and address of the organization(s) financially responsible for and monitoring the work.

10. SPONSOR/MONITOR'S ACRONYM(S). Enter, if available, e.g. BRL, ARDEC, NADC.

11. SPONSOR/MONITOR'S REPORT NUMBER(S). Enter report number as assigned by the sponsoring/ monitoring agency, if available, e.g. BRL-TR-829; -215.

12. DISTRIBUTION/AVAILABILITY STATEMENT. Use agency-mandated availability statements to indicate the public availability or distribution limitations of the report. If additional limitations/ restrictions or special markings are indicated, follow agency authorization procedures, e.g. RD/FRD, PROPIN, ITAR, etc. Include copyright information.

13. SUPPLEMENTARY NOTES. Enter information not included elsewhere such as: prepared in cooperation with; translation of; report supersedes; old edition number, etc.

14. ABSTRACT. A brief (approximately 200 words) factual summary of the most significant information.

15. SUBJECT TERMS. Key words or phrases identifying major concepts in the report.

16. SECURITY CLASSIFICATION. Enter security classification in accordance with security classification regulations, e.g. U, C, S, etc. If this form contains classified information, stamp classification level on the top and bottom of this page.

17. LIMITATION OF ABSTRACT. This block must be completed to assign a distribution limitation to the abstract. Enter UU (Unclassified Unlimited) or SAR (Same as Report). An entry in this block is necessary if the abstract is to be limited.

Report Type: Final Report

Primary Contact E-mail: cklaw@princeton.edu

Primary Contact Phone Number: 609-258-5271

Organization /Institution name: Princeton University

Award Information

Grant/Contract Title: PHYSICAL AND CHEMICAL PROCESSES IN TURBULENT FLAMES

Grant/Contract Number: FA9550-13-1-0119

Principal Investigator Name: Prof. Chung K. Law

Program Manager: Dr. Chiping Li

Report Information: Final Report

Reporting Period Start Date: March 15, 2013

Reporting Period End Date: March 14, 2015

Report Abstract

The two-year subject program, conducted through tight coupling between experiment, theory and computation, and reported in high impact journal articles, has focused on the dynamics of turbulent flames mainly for hydrocarbon fuels in environments simulating various operational aspects of aero-engines. The thrust for this program constitutes of three major areas of turbulent combustion: (1) Flame surface statistics, (2) Flame-turbulence interaction, and (3) Effects of turbulence on the growth of ignition kernel.

Using high-speed Mie-scattering we investigated the local flame surface statistics of constant-pressure turbulent expanding flames. First, the statistics of the local length ratio is experimentally determined from high-speed planar Mie scattering images of spherically expanding flames, with the length ratio on the measurement plane, at predefined equiangular sectors, defined as the ratio of the actual flame length to the length of a circular-arc of radius equal to the average flame radius. Assuming isotropic distribution of such flame segments we then convolute suitable forms of the length-ratio probability distribution functions (*pdf*s) to arrive at the corresponding area-ratio *pdf*s. It is found that both the length ratio and area ratio *pdf*s are near log-normally distributed and shows self-similar behavior with increasing radius.

To quantify the effect of the flame on the turbulence the mean and the *rms* of the flow field are measured over a range of conditions both in the presence and absence of the flame using High Speed PIV. The distributions of stretch rate contributions from different terms such as tangential straining, normal straining and curvature are also obtained. It is found that the normal straining displays non-Gaussian *pdf* tails whereas the tangential straining shows near Gaussian behavior. We have further tracked the motion of the edge points that reside and co-move with the edge of the flame kernel during its evolution in time, and found that within the measurement conditions, on average the persistence time scales of stretch due to pure curvature exceed those due to tangential straining by at least a factor of two.

Finally we experimentally demonstrated that contrary to the belief that ignition of a combustible mixture by a high-energy kernel is more difficult in turbulence than in quiescence because of the increased dissipation rate of the deposited energy, it can actually be facilitated by turbulence for mixtures whose thermal diffusivity sufficiently exceeds its mass diffusivity. In such cases, turbulence breaks the otherwise single spherical flame of positive curvature, and hence positive aerodynamics stretch, into a multitude of wrinkled flamelets possessing either positive or negative stretch, such that the intensified burning of the latter constitutes local sources to facilitate ignition.

1. Experimental Setup:

All the experimental studies reported here used a constant-pressure, fan-stirred combustion chamber to investigate the propagation of a spherically expanding flame (Fig. 1.1). Chambers based on this design have been used to study various aspects of laminar and turbulent expanding flames, and are detailed in our previously published articles [Tse et al (2004), Kelly and Law (2009), Chaudhuri et al (2012)]. Briefly, the apparatus consists of two cylindrical chambers: an outer chamber that houses an inner chamber of a much small volume and an almost unity aspect ratio (Inner dia: 114 *mm*; outer dia: 167 *mm*; length: 127 *mm*). The flat ends of the inner chamber are sealed with thick quartz windows for optical access. The inner chamber is filled with the test fuel/air mixture which is spark-ignited, while the outer chamber is filled with an inert of the same pressure. The connection between the chambers is controlled by four valves (sliding sleeve with multiple holes) that are opened at the instance of the spark discharge, hence allowing the expanding flame to come in contact with the inert in the outer chamber and instantly quench. The expansion process, thus, is nearly isobaric owing to the small volume of the inner chamber compared to that of the outer chamber. Experiments up to the range of 30 to 60 *atm* have been conducted based on this dual-chamber design, although the maximum pressure for the current experiments was kept to 5 *atm* as it is sufficient for the present study.

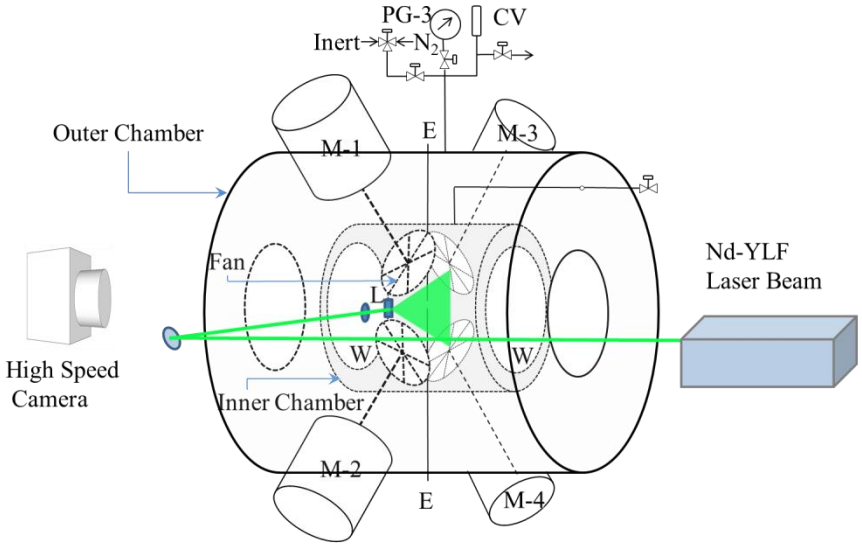

Experimental Setup. CV: Check Valve, PG: Pressure Gauge, PT: Pressure Transducer, M: Fan Motor, L: Cylindrical Lens, E: Electrodes, W: Quartz Window

Fig. 1.1: experimental setup with all the components.

The turbulence in the chamber is generated using four equally spaced continuously running fans (69 *mm* diameter), powered by motors enclosed in the outer chamber. The motors are controlled by using a feedback mechanism, which regulates the power of the motors to maintain constant speed.

To detect the flame edge during the combustion process we seed the air using DEHS droplets (nominal diameter ~ 1-2 μm) generated by a high-pressure nebulizer. A high-speed Nd-YLF laser (527 *nm*) synchronized with a high-speed camera (Phantom v7.3) is used for Mie scattering. Using beam expanding optics the 2 *mm* diameter laser beam is expanded to a 750 μm thick laser sheet inside the inner chamber as shown in the figure. The camera placed at 90^o from the laser plane recorded the event at 8000 *fp*s with a resolution of 608×600 to achieve a spatial resolution of ~50 μm/pixel. Before ignition the entire chamber remains filled with droplets showing a uniform distribution of seed density. Following ignition, as the flame propagates the seeding droplets inside the flame vaporize, hence limiting the high seeding density only outside the flame (Fig. 2bi). Post processing the high-speed images, the instantaneous 2D flame (on the laser plane) edge (the edge of the seeding concentration) was detected using Canny edge detection technique through Matlab. During image processing we mask the electrodes to avoid their influence of the statistics.

2. Flame Surface Statistics:

Turbulent flame speed is a major topic of sustained interest in turbulence and combustion research. Starting with Damköhler`s pioneering work [Damköhler 1940], it is generally believed and shown by many studies that, at least for equidiffusive mixtures, the turbulent flame speed is largely controlled by the total flame surface area, with the normalized turbulent flame speed assumed proportional to the normalized flame surface area. Since the turbulent flame speed is a global statistics, it is of interest to consider how the distribution of quantities related to the local flame surface, such as the flame surface area ratio, build up this global measure. The turbulent flame surface is typically highly wrinkled and folded over a multitude of scales, starting from the hydrodynamic length scale to the smallest scales controlled by the Kolmogorov length scale and flame properties such as the Markstein length and flame thickness. Therefore it is useful if the information contained in this complex geometry can be projected onto a simple regular geometry such as a plane or a smoothly curved surface. A straightforward way to arrive at this simple geometry is to just consider a filtered/average location of the flame positions to represent a smooth surface. The information contained in the wrinkled surface if projected on this simple geometry will also make it amenable for well-known processing techniques such as spectral, wavelet or multifractal analysis. Not only such an approach would be useful for analysis but it might be also of interest in reduced-order modeling, such as Large Eddy Simulation or Reynolds Averaged Navier-Stokes Equation, in which very fine scale flame surface wrinkling and the information contained therein cannot be directly simulated due to limitation of the resolution. By this approach the wrinkled surface information randomly distributed in three dimensions (volume) is now described using two dimensions (a regular surface), essentially resulting in a reduction of the dimensionality of the problem. The knowledge of the local area ratio is also pivotal in obtaining the Probability Distribution Functions (*pdf*s) of any quantity conditioned on that surface. Motivated by its importance for both fundamental understanding and reduced-order simulation of turbulent flames, this work focuses on the local statistics of flame surface area.

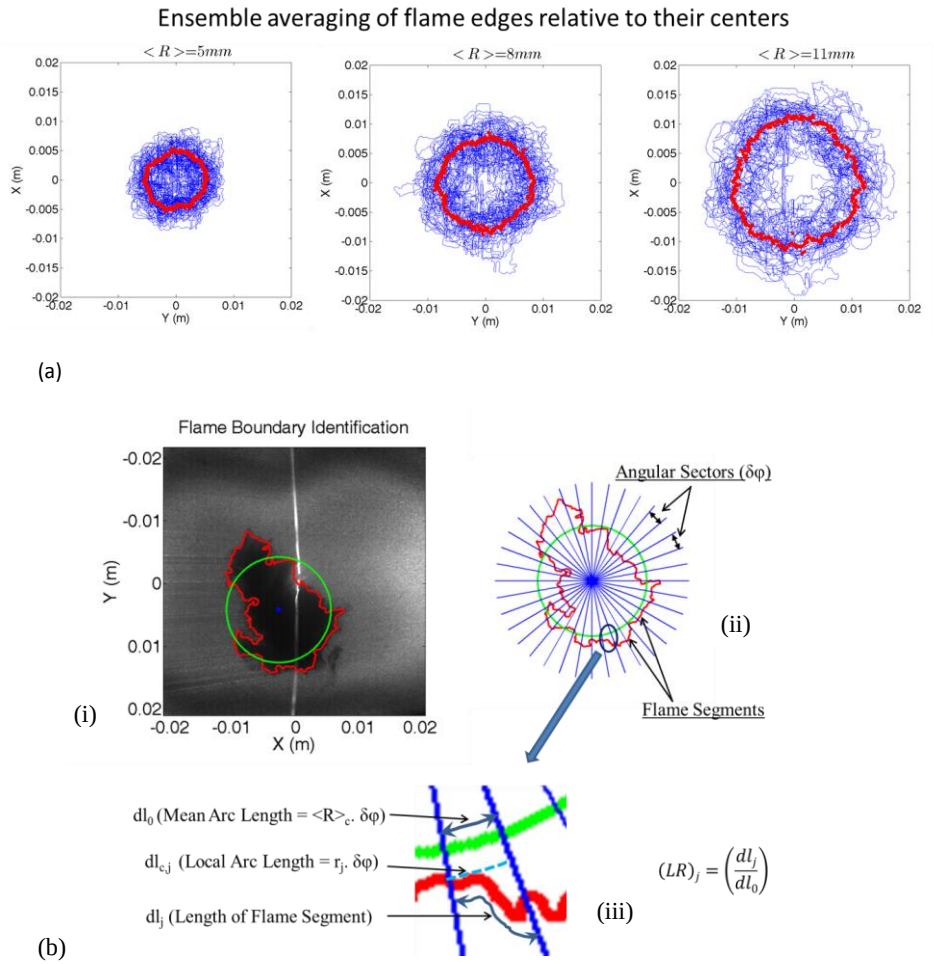

Fig. 2.1 (a) This figure shows instantaneous realizations of the flame edges (blue lines) at the same $<R>$ for all the conditions and runs. The thick red line shows a curve obtained by ensemble averaging of instantaneous flame edges at each angular sector. (b) This image demonstrates the procedure of extracting the length ratio statistics from Mie scattering images. (i) A typical Mie scattering image. Red line shows the flame edge, green line shows the circle with mean radius $<R>_c$. (ii) Extracted flame edge broken down to angular sectors. (iii) In an angular sector the important measurements, dl_0, dl_c and dl_j. It is important to note that in this sector the flame edge overcuts the mean circle (*i.e.*, the flame edge is at the higher radial location). However, in some angular sectors it can undercut the mean circle. Thus, the quantity $(LR)_j$ can locally have values less than unity.

Using the G-equation and starting with the flame surface area ratio, Kerstein et al. (1988) obtained an expression for the turbulent flame speed of a statistically planar flame, propagating in the **i** direction in the mean. The projected area of such a propagating flame surface, *i.e.* the *y-z* plane, was divided in equal infinitesimal areas $dA_0 = dydz$. Consequently, if the local flame surface area contained within a cylinder of cross sectional area dA_0 with the axis parallel to **i** is

given by $dS(G_0)$, where $\mathbf{i}$ is the unit normal in *x*-direction with the flame being represented by a level set $G = G_0$, then the turbulent flame speed can be expressed as:

$$\frac{S_T}{S_L} = \frac{A_T}{A_0} = \left\langle \frac{dS(G_0)}{dA_0} \right\rangle \tag{2.1}$$

It was recognized that due to folding of the flame surface $G = G_0$, multiple flame segments might be encountered within a given cylinder. Each of these segments referenced by index *j* was considered locally planar with local surface normal represented by $\mathbf{n}_j$. Then the area ratio for the j^{th} segment is given by $dS(G_0)_j / dA_0 = 1/\left|\mathbf{i}\bullet\mathbf{n}_j\right|$ and the flame area contained within the cylinder is given by summing over *j*:

$$dS(G_0)/dA_0 = \sum_j 1/\left|\mathbf{i}\bullet\mathbf{n}_j\right|. \tag{2.2}$$

Correspondingly, for an expanding flame which is nearly spherical (from experiments reported in the following) on ensemble averaging, as shown in Fig. 2.1a, a sphere with radius equal to the average radius of the flame can be considered to be the base or projected surface. This projected surface can be decomposed into infinitesimal area elements $dA_s = \langle R\rangle_s^{\,2} \sin\theta d\theta d\phi$, where $\langle R\rangle_s$ is the average radius, the polar angle ϕ and the azimuthal angle θ. To assess the ratio of the actual flame surface with the projected area, we consider imaginary tetrahedral cones whose apex is the center of the sphere and has cross-sectional area dA_s where it intersects the projected surface (as shown in Fig. 1b). The wrinkled flame area contained within a cone can be represented by $dS_s(G_0)$. In our experiments, measurements are performed using 2D Mie-scattering technique at the laser plane, hence the above discussion should be modified for a planar case where the projected contour is a circle and the infinitesimal projected length element is given by $dl_0 = \langle R\rangle_c \, d\phi$. In the above the subscripts *s* and *c* represent spherical (3D) and circular (2D) projections respectively. The corresponding length ratio contained within each of the sectors is given by

$$dl(G_0)/dl_0 = \sum_j \left(1/\left|\mathbf{r}_j\bullet\mathbf{n}_j\right|\right)\left(r_j/\langle R\rangle_c\right). \tag{2.3}$$

Here $\mathbf{r}_j$ is the unit normal in the radial direction and the second factor arises due to change in length of the circular segment between the local radius r_j and average radius $\langle R\rangle_c$. Summation over j is still important as the flame edge determined can be folded, resulting in multiple flame segments crossing within a given sector. Schematic of the determination of such a length ratio is

shown in Fig. 1b. Now the flame edge that we obtain can be represented by the level set $G = G_0$, with

$$\mathbf{n}_j = \nabla G_{G=G_0} / \left|\nabla G\right|_{G=G_0} \tag{2.4}$$

Hence Eq. (2.2) can be rewritten as:

$$dl\left(G_0\right) / dl_0 = \sum_j \left(\left|\nabla G\right|_{G=G_0} / \left|\mathbf{r}\bullet\nabla G\right|_{G=G_0} \right) \left(r_j / \left\langle R \right\rangle_c \right) \tag{2.5}$$

which in $r-\phi$ coordinates is given by,

$$dl\left(G_0\right) / dl_0 = \sum_j \sqrt{1+\left(\frac{1}{r}\frac{\partial G}{\partial \phi}\right)^2 \Big/ \left(\frac{\partial G}{\partial r}\right)^2} \left(\frac{r_j}{\left\langle R \right\rangle_c} \right) \tag{2.6}$$

i.e. in this 2D realization any surface fluctuation in the out-of-plane direction (here θ) is neglected. In particular the actual area ratio in the $r-\phi-\theta$ spherical coordinates is given by:

$$dS\left(G_0\right) / dA_0 = \sum_j \sqrt{1+\left(\frac{1}{r}\frac{\partial G}{\partial \phi}\right)^2 \Big/ \left(\frac{\partial G}{\partial r}\right)^2 + \left(\frac{1}{r\sin\phi}\frac{\partial G}{\partial \theta}\right)^2 \Big/ \left(\frac{\partial G}{\partial r}\right)^2} \left(\frac{r_j}{\left\langle R \right\rangle_s} \right)^2 \tag{2.7}$$

We will discuss shortly that using statistical methods and some assumptions about the corresponding distributions one can arrive at the 3D area ratio statistics from the measured 2D length ratio statistics. While extrapolation from 2D statistics to 3D statistics is not straightforward, it can be certainly expected that:

$$\frac{S_T}{S_L} = \left\langle \frac{dS\left(G_0\right)}{dA_0} \right\rangle \neq \left\langle \frac{dl\left(G_0\right)}{dl_0} \right\rangle \tag{2.8}$$

Recognizing this, we propose a systematic method for converting the 2D length ratio statistics to the 3D area ratio statistics. In doing this we assume: i) the statistics of the surface are invariant upon rotation; and ii) the in-plane and out-of-plane statistics are mutually independent. Consequently, we can utilize the *pdf* of the second term in the RHS of Eq. (2.7) to generate the *pdf* of the corresponding third term. Then we need to generate a *pdf* of the sum of these two terms which can be done by convoluting the two *pdf*s as shown below.

Let X and Y be two discrete and independent random variables with $Z = X + Y$ as the sum of the two random variables. Then the events $X = a$ and $Z = c$ can only occur simultaneously if $Y = c - a$. Since X and Y are independent, the probability of $Z = c$ is thus given by convolution of the probabilities $X = a$ and $Y = c - a$,

$$P(Z=c)=\sum_{a=-\infty}^{\infty} P\left(X=a\right)\cdot P\left(Y=c-a\right) \tag{2.9}$$

Through edge detection technique used on 2D Mie-scattering images, the instantaneous flame edge can be extracted as shown in Fig.2.1b (ii). It is to be noted that the flame edge at any instance is representation of the level set function $G = G_0$. The figure also shows the circle (centered at the centroid of the area under flame edge) with a mean radius $\langle R\rangle_c$. The flame edge has been divided into small angular sectors of 1^o each. Through image processing technique we calculate or evaluate the ratio of the flame edge length to the arc length of a mean circle ($dl(G_0)/dl_0$) as shown in Fig. 2.1.b (iii). Due to stretching, wrinkling and folding under turbulence it is possible that the flame edge can have multiple cuts or segments in one sector. Although the number of segments in each sector can be different, each sector will have at least one flame segment.

Now, following Eq. (2.6), for the j^{th} flame segment at the i^{th} sector we can write,

$$\left[dl\left(G_0\right)/dl_0\right]_{i,j}=\sqrt{1+\left(\frac{1}{r}\frac{\partial G}{\partial \phi}\right)^2\Big/\left(\frac{\partial G}{\partial r}\right)^2}\left(\frac{r_j}{\langle R\rangle_c}\right) \tag{2.10}.$$

We next define a parameter $U_{i,j}=\left(\frac{r_{i,j}}{\langle R\rangle_c}\right)^4\left[\left(\frac{1}{r}\frac{\partial G}{\partial \phi}\right)^2\Big/\left(\frac{\partial G}{\partial r}\right)^2\right]_{i,j}$ which can be evaluated for any value of i and j using

$$\left(\frac{r_{i,j}}{\langle R\rangle_c}\right)^4\left[\left(\frac{1}{r}\frac{\partial G}{\partial \phi}\right)^2\Big/\left(\frac{\partial G}{\partial r}\right)^2\right]=\left[\left(\frac{\langle R\rangle_c}{r_j}\left[dl\left(G_0\right)/dl_0\right]_{i,j}\right)^2-1\right]\left(\frac{r_{i,j}}{\langle R\rangle_c}\right)^4. \tag{2.11}$$

From the statistics of $U_{i,j}$, it is possible to obtain a probability distribution function for the j^{th} segment *i.e.* $pdf\left[U_j\right]$.

Now if we assume that the statistics of the surface are invariant upon rotation, *i.e.* the surface is isotropic, we can say experiments on a plane rotated by 90^o [r-θ plane], the statistics of the quantity $\left(\frac{1}{r}\frac{\partial G}{\partial \theta}\right)^2\Big/\left(\frac{\partial G}{\partial r}\right)^2$ would have been similar to the statistics of $\left(\frac{1}{r}\frac{\partial G}{\partial \phi}\right)^2\Big/\left(\frac{\partial G}{\partial r}\right)^2$ obtained for the current experimental plane (r-φ plane) or

$$pdf\left[\left(\frac{r_j}{\langle R\rangle_c}\right)^4\left[\left(\frac{1}{r}\frac{\partial G}{\partial \theta}\right)^2\Big/\left(\frac{\partial G}{\partial r}\right)^2\right]\right]_j=pdf\left[\left(\frac{r_j}{\langle R\rangle_c}\right)^4\left[\left(\frac{1}{r}\frac{\partial G}{\partial \phi}\right)^2\Big/\left(\frac{\partial G}{\partial r}\right)^2\right]\right]_j=pdf\left[U_j\right] \tag{2.12}.$$

Now as we know the statistics that sinφ is based on, we can also obtain $pdf\left[Y_j\right]$, where

$$Y_{i,j}=\left(\frac{r_{i,j}}{\langle R\rangle_c}\right)^4\left[\left(\frac{1}{r\sin\varphi}\frac{\partial G}{\partial\theta}\right)^2\Big/\left(\frac{\partial G}{\partial r}\right)^2\right]_{i,j} \tag{2.13a}$$

Following the definition of *U*, we define a second parameter

$$X_{i,j}=\left(\frac{r_{i,j}}{\langle R\rangle_c}\right)^4\left[1+\left(\frac{1}{r}\frac{\partial G}{\partial\phi}\right)^2\Big/\left(\frac{\partial G}{\partial r}\right)^2\right]_{i,j} \tag{2.13b}$$

and calculate the probability distribution function for the j^{th} segment, *i.e*, $pdf\left[X_j\right]$.

Using our second assumption that the statistics on the *r*-φ plane and *r*-θ plane are mutually independent, we can use the convolution between $pdf\left[X_j\right]$ and $pdf\left[Y_j\right]$ to arrive at $pdf\left[X_j+Y_j\right]$. Now we define $Z_j=X_j+Y_j$, and perform successive convolution on $pdf\left[\sqrt{Z_j}\right]$ for all possible values of *j*, we arrive at

$$pdf\left[dS\left(G_0\right)/dA_0=\sum_j\sqrt{Z_j}\right]. \tag{2.14}$$

In the following, we first briefly discuss the length ratio *pdf*s and then the area ratio *pdf*s in more detail, for unity Lewis number (*Le*), CH_4-air, $\phi=0.90$ flames at two levels of turbulence intensity (u_{rms} = 1.43 and 2.85 *m/s* with fan speed = 2000 and 4000 *rpm*, respectively) and at three different pressures (*p* = 1, 2 and 5 *atm*). The Markstein numbers (*Mk*) obtained from laminar expanding flame experiments for mixture conditions corresponding to the present turbulent experiments are nearly constant, slightly decreasing with pressure from 1.18 to 0.73. We also include a *Le* > 1 case: C_4H_{10}-air, ϕ = 0.8 (u_{rms} = 1.43 *m/s* (fan speed = 2000 *rpm*), *p* = 5 *atm*, *Mk* = 2.75) to qualitatively assess the importance of *Mk* on the flame surface area ratio statistics.

We next study the flame length ratio obtained directly from the experiments, without any assumption. As explained earlier (Eq. 2.8) the length ratio, ($LR=dl(G_0)/dl_0$) is not equivalent to the area ratio, ($AR=dl(G_0)/dl_0$), which is directly related to the flame speed. Nevertheless, the mean of this scalar quantity should follow similar characteristics as the flame burning flux which increases with pressure, turbulence intensity, and in general with the turbulence Reynolds number. Moreover, with the current experimental procedure being 2D in nature, the length ratio is the most fundamental parameter of interest, denoting the projection of the 2D flame edge on the mean circle. Since turbulence wrinkles the flame to destroy its smooth spherical shape that

one can observe in laminar experiments, the length ratio is thus a direct measure of the extent of flame wrinkling.

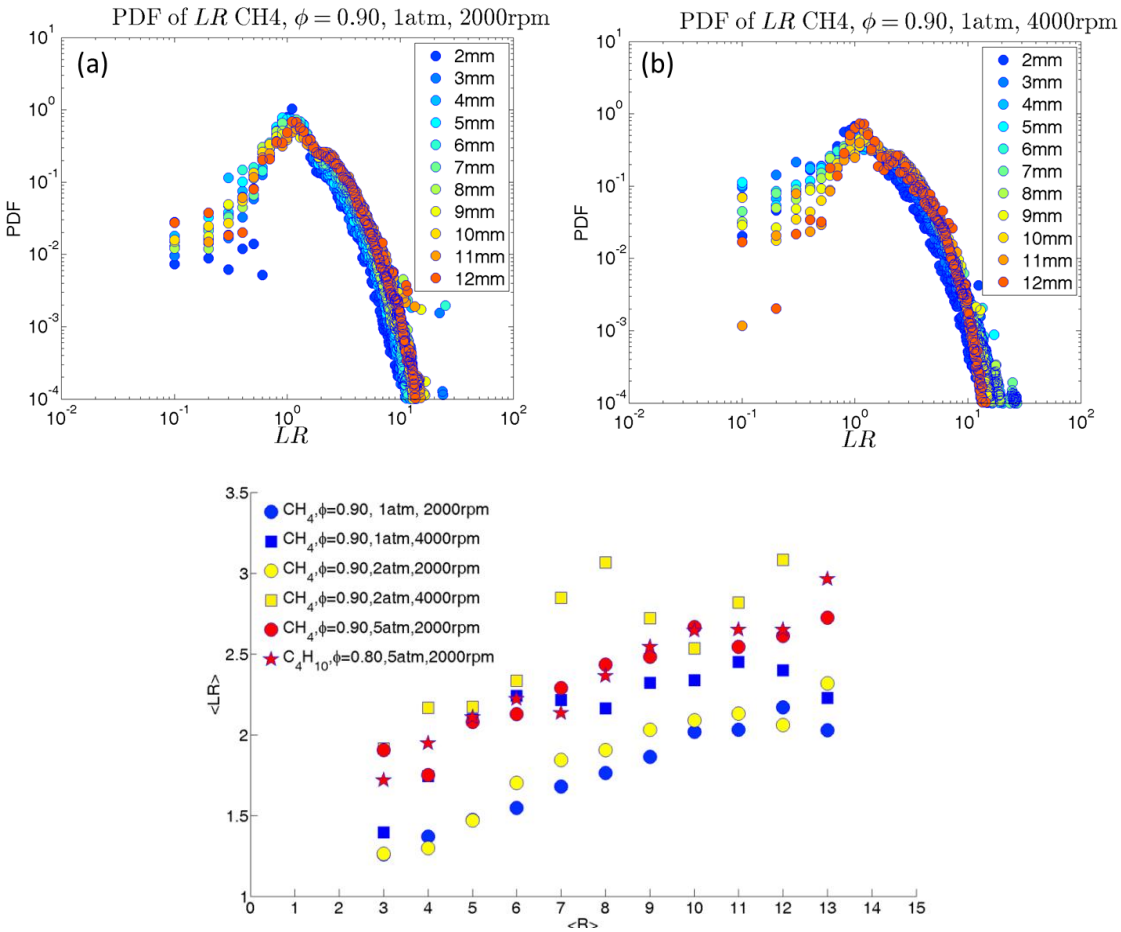

Fig. 2.2: Evolution of length ratio *pdf*s with the flame radius <*R*> (*mm*) for CH_4 flame: *a) 1atm, 2000rpm, b) 1 atm, 4000 rpm and c) Evolution of <LR> with the flame radius <R> (mm) for different CH_4 flame at different pressure and rpm*

Figure 2.2 shows the probability density functions (*pdf*s) for two different conditions at different mean radii. The first observation that emerges from these *pdf*s is that they display a somewhat distorted log-normal nature. Physically such a distribution signifies that the length ratio can attain extreme values with wide separations, which is an inherent nature of a dissipative quantity under turbulence, due to its multiplicative randomness. Secondly, it is also evident that, despite its similarity in the shape, the distribution at any condition shifts to the right with the radius. This shift can be captured more effectively with the mean *LR* (<*LR*>) plotted in Fig. 2.2e, which shows a clear increase with radius. This increase signifies that the flame becomes more and more strained and wrinkled as is expands, which in turn ensures an increase in the turbulent flame speed. Higher turbulence intensities increase the small structures in the flame edge, making the flame more wrinkled. This is reflected as the increase in <*LR*> when we compare the CH_4 flames under the same pressure but two different turbulence intensities (Fig. 2.2e). Although the

turbulence promotes wrinkling and stretching of the flame edge, they are also being inhibited by Markstein diffusion which prevents the evolution of small-scale structures. The effect of Markstein diffusion and its influence on turbulent flame wrinkling is not very clear from the <*LR*> values of the CH_4 and C_4H_{10} flames at 5 *atm*, 2000 *rpm*, where the latter has larger Markstein numbers. The plot (Fig. 2.2e) shows that both flames have very similar length ratios making it difficult to distinguish the effect of the Markstein number. We recognize that at higher pressures (such as 5 *atm*) the smallest scales of flame surface wrinkling may be near or below the limit of imaging resolution, barring proper reconstruction of the local length ratio. Higher resolution imaging is necessary to clarify such differences at these pressures. We will however also show later that this influence of the Markstein number becomes clearer when we compare the area ratio statistics.

We also have computed the area ratio quantities, as AR directly correlate with the turbulent flame speed. Figure 2.3 compares the Area Ratio *pdf*s for two different conditions. Although the shape of the pdfs for *LR* and AR are similar, the mean of these quantities are different. As explained in Eq. (2.1), the mean <*AR*> is representative of the flame speed, which is shown in Fig. 2.3c. Clearly, the values of <*AR*> are quite different from those of <*LR*> presented in Fig. 2.2c. This therefore demonstrates that the 2D measurement of the length ratio cannot readily represent the normalized turbulent flame speed before applying this or other equivalent conversion. The values of the area ratio presented in Fig. 7, on the other hand are obtained from a 3D statistics, and as such can be used to represent the normalized flame speed. The comparative study of Fig. 2.3c shows some fundamental characteristics of the flame surface under turbulence. As explained earlier, the flame surface undergoes extensive stretching, wrinkling and folding in the presence of turbulence. Due to the multiplicative nature of randomness, the area ratio shows a near log-normal distribution which is a common signature of a dissipative scalar in strong turbulence. For a turbulent expanding flame the hydrodynamic length scale increases with flame size which is an artifact of increased flame brush thickness or the volume that the wrinkled flame occupies. In other words, as the flame expands, it becomes more wrinkled resulting in an increase in <*AR*> as seen in Fig. 2.3c. As observed for the length ratio, the area ratio also increases with the turbulence intensity due to intense stretching and folding of the flame [Fig. 7 (CH_4 flames: 1 *atm* (2000, 4000 *rpm*) and 2 *atm* (2000, 4000 *rpm*)]. The effect of Markstein diffusion on the other hand becomes apparent while comparing the 5 *atm* flames of CH_4 and C_4H_{10}, in which the former shows higher values of <*AR*> due to more wrinkling of the flame compared to C_4H_{10}, which has a higher Markstein number.

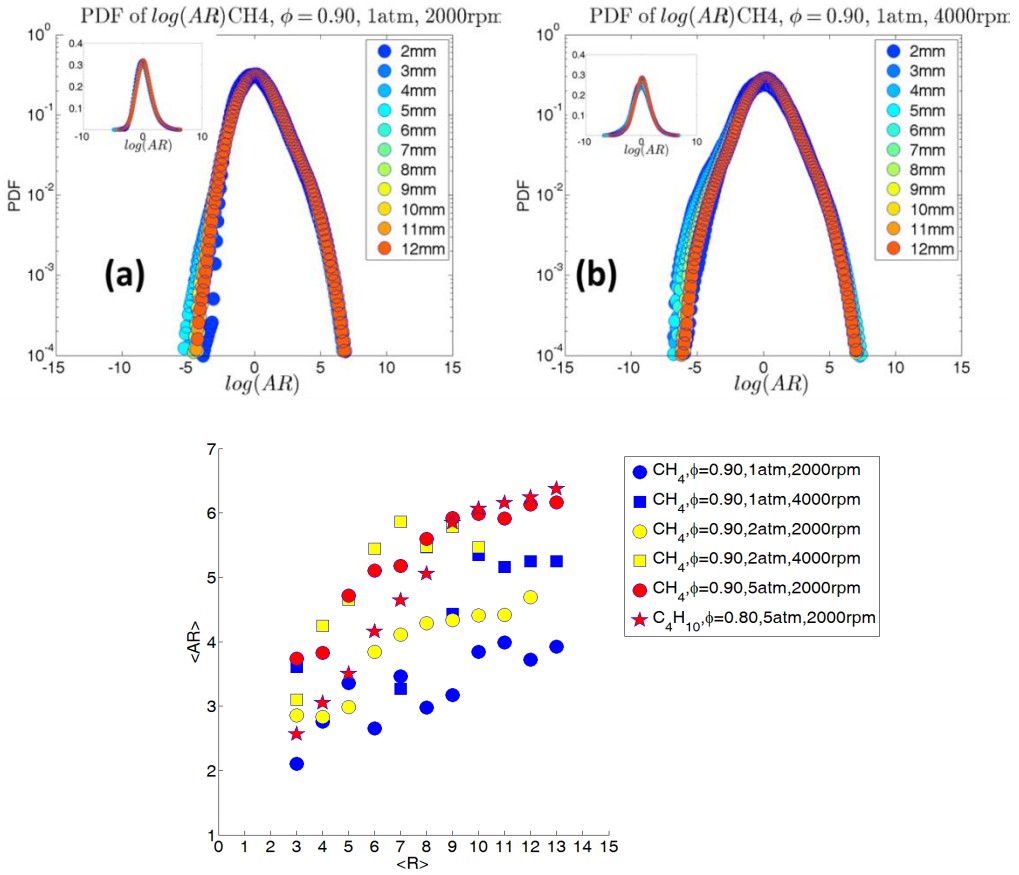

Fig. 2.3: Evolution of normalized Area ratio *pdf*s with the flame radius <*R*> (*mm*) for CH_4 flame (linear Y scale in inset): *a) 1 atm, 2000 rpm, b) 1 atm, 4000 rpm, and c) Evolution of <AR> with the flame radius <R> (mm) for different CH₄ flame at different pressure and*

3. Flame-Turbulence Interaction

This part of the study focuses on the interaction between turbulence on flames and vice versa. The fundamental parameters that quantify the state of turbulence, if it is nearly isotropic, are the turbulence intensity u_{rms} and the integral length scale L_I. The quantities that characterize the local flame structure are the local laminar flame speed $\tilde{S}_L$ and flame thickness δ_L. According to the hydrodynamic theory of premixed flames the stretched laminar flame speed $\tilde{S}_L$ is given by:

$$\tilde{S}_L = S_L - \delta_M \mathbf{K} \tag{3.1}$$

where S_L and δ_M are the planar laminar flame speed and Markstein length respectively 0, $\mathbf{K}$ is the total stretch rate which can be further decomposed as 0:

$$\mathbf{K} = \overbrace{S_L\kappa}^{\text{stretch rate by curvature: } K_\kappa} - \underbrace{(\mathbf{v}\cdot\mathbf{n})\kappa}_{\text{normal strain: } K_n} + \nabla_t \cdot \mathbf{v}_t \quad , \tag{3.2}$$

$S_L\kappa$: stretch rate by pure curvature: K_c; $\nabla_t \cdot \mathbf{v}_t$: tangential strain: K_t

in which $K_t = \left(\delta_{ij} - n_i n_j\right) S_{ij}$, and $\delta_{ij} = 1$ for $i = j$; 0 for $i \neq j$; with S_{ij} being the strain rate tensor. The second and third terms on the RHS of Eqn. (3.2) together is the stretch rate contribution by the strain rate, K_s. Stretch rates originating from the tangential strain rate K_t, normal strain K_n and stretch due to pure curvature K_c can be considered to be parameters that quantify the turbulence-flame interaction as well 0. In general, turbulence results in multi-scale wrinkling of the flame surface, affecting the aerodynamics of the flame which in turn affects the nearby flow field by heat release and gas expansion. Since the burned products in the expanding flame should be statistically stationary, the flame could induce a mean outward flow that might affect the turbulence parameters like u_{rms} and L_I in the otherwise cold non-reacting flow. It appears that in all experimental efforts on turbulent expanding flames only cold flow turbulence parameters like u_{rms} and L_I measured in the absence of flame have been reported. It is thus critical to investigate to what degree these fundamental quantities are affected, if at all, by the flame as these modified parameters are what distort the flame instead of the quantities measured in its absence.

In view of such a need, we attempted to provide experimental high-speed particle image velocimetry data that quantifies flame-turbulence interaction dynamics well resolved in two dimensional space and time, as the flame evolves from a wrinkled flame kernel to a well-developed expanding turbulent flame. The high-speed Mie scattering which is a necessary precursor to HS-PIV allows us to extract the flame edges from the maximum seed density gradients. This enables tracking the evolution of the curvature statistics. The flow velocity and strain rate tensor components from the HS-PIV could be superposed on these flame edges, allowing investigation of the evolution of stretch rate statistics due to both local strain rate and curvature.

Figures 3.1a and 3.1b show the mean radial velocity $\langle U_r \rangle$ and the effective turbulent intensity on the flame $u'_{eff} = \overline{\left[\frac{1}{2}\left(\left\langle \left(u_x - \langle u_x \rangle_R\right)^2 \right\rangle_R + \left\langle \left(u_y - \langle u_y \rangle_R\right)^2 \right\rangle_R\right)\right]^{1/2}}$ for all the cases under study, respectively. We also compared these results with those obtained from the corresponding cold flow measurements in the absence of flame, prior to ignition. We observe that in the absence of the flame the mean radial flow is directed inward (towards the center of the chamber) indicated by the negative values in Figure 3.1a. This weak radial flow also increases with radius, closer to the fans. However during flame expansion, the mean radial flow adjacent to the flame is radially outward in nature shown by the positive values of $\langle U_r \rangle$. As the flame expands it pushes the unburnt gas in front of it. This effect becomes stronger as the flame accelerates with increase in radius, resulting in increasing $\langle U_r \rangle$ with $\langle R \rangle$. However, we found that there is no discernible change in the u'_{eff} in the presence of the flame. This shows the effect of flame on turbulence intensity is rather weak.

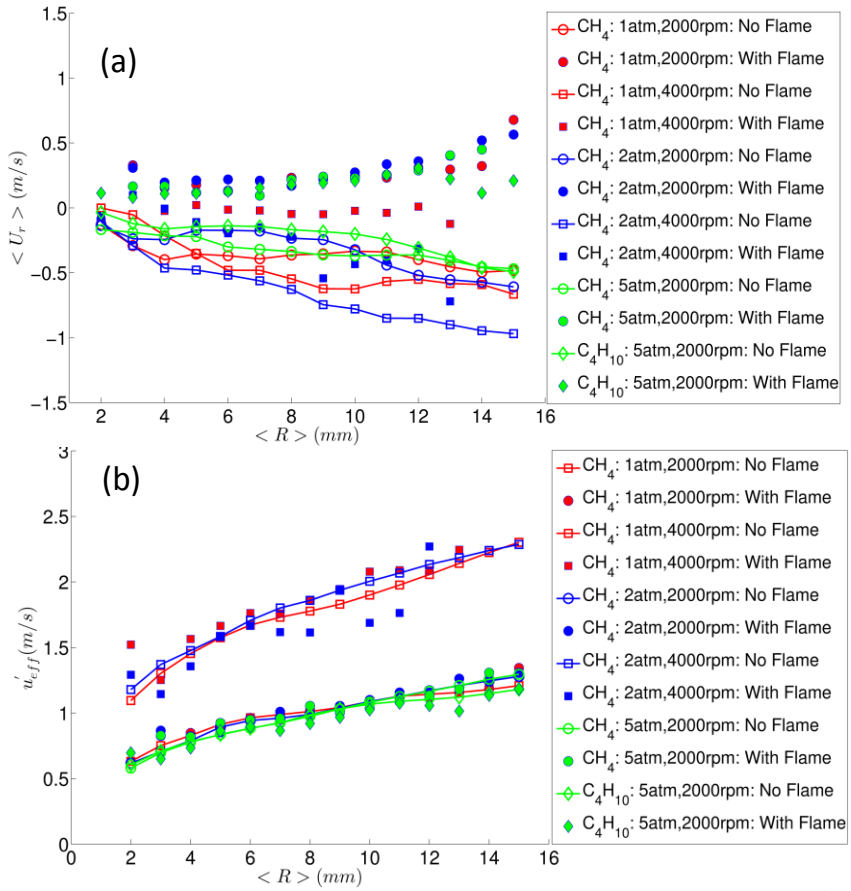

Fig. 3.1: *Plot of (a) ensemble averaged <U_r> vs <R> and (b) ensemble averaged u'_{eff} vs. <R> in presence and in absence of flame*

In Figure 3.2 we look into the evolution of the probability distribution functions (*pdf*s) for K_t and K_n defined in Eqn. (3.2). The *pdf*s are computed over the ensemble of all the runs for a given condition, conditioned at particular values of $\langle R \rangle$. It is clearly seen that both the K_t and K_n show self-similar profiles during their evolution with $\langle R \rangle$. However, when plotted on a log scale the nature of the *pdf* tails of K_t and K_n appear different. The *pdf* for K_t shows parabolic tails suggesting Gaussian distribution, whereas K_n shows non-Gaussian stretched tails implying finite probability of very large K_n values in comparison to its near Gaussian counterpart K_t. Clearly with increase in u_{rms} both the K_t and K_n *pdf* tails are flared. As the turbulence Reynolds number Re_T increases (with turbulence intensity), the Kolmogorov length scale η decreases, resulting in the emergence of smaller scale eddies which are also highly strained and intermittent. These impart larger K_t and K_n observed from the flaring of the tails. It is also important to see if the increased u_{rms} or Re_T has similar impact on the mean stretch rates in addition to that on the higher moments.

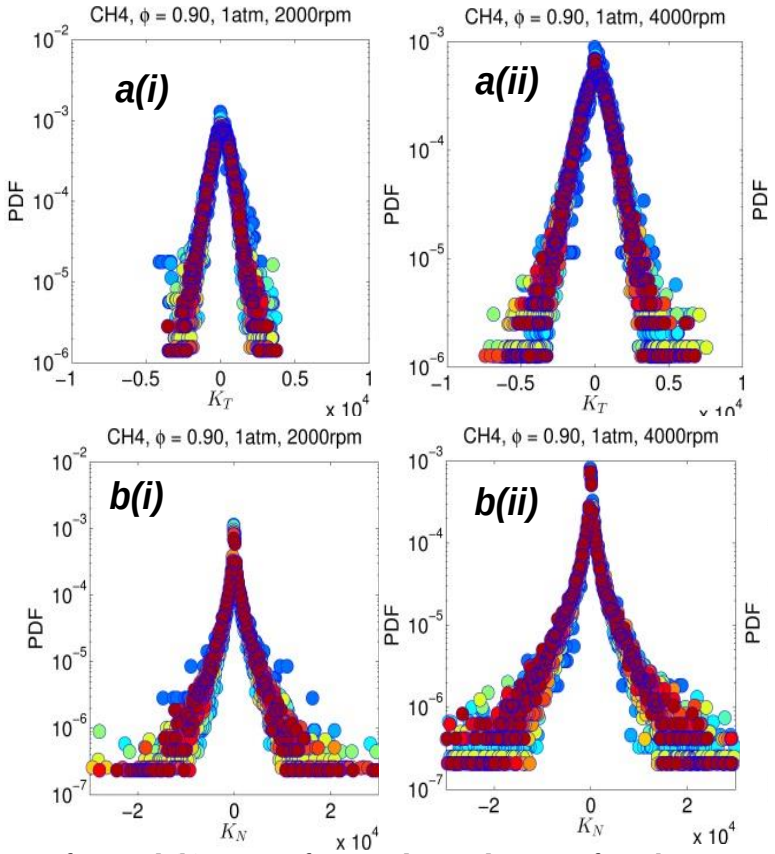

Fig. 3.2 *: (a) PDFs of K_t and (b) PDFs of K_n conditioned at specific values <R>, over six different conditions of fuel-air mixtures, u_{rms} and pressure: (i) CH_4: 1atm and 2000rpm, (ii) CH_4: 1atm and 4000rpm*

Recently Clavin and GrañOtero 0 analytically showed the existence of two unique Markstein lengths, one due to strain rate and the other due to curvature. Following the same notion, if one can isolate the persistence time scales of these two Markstein lengths, it is possible to distinguish between their relative importance and to assess the relative relevance of local strain and local curvature for dissipating turbulent flame surface fluctuations. From a modelling point of view this is of considerable interest especially in the context of G-equation used for the description of a premixed flame [Peters (1999)]. Currently, to describe the response of flame speed to unsteady stretch, expected in turbulent flows, two limiting conditions are typically used. The first approach is to consider Markstein lengths obtained in steadily stretched flames **Error! Reference source not found.** and the second approach is to consider vanishing effect of Lewis number (*Le*) under overwhelming presence of turbulent transport say in thickened flamelet regimes **Error! Reference source not found.**. It is possible that for wide conditions of interest in moderate to large turbulence Reynolds numbers $\left(\mathrm{Re}_T > 100\right)$ and intermediate Damköhler numbers $\left(0.1 < Da < 10\right)$ the flame response to stretch is somewhat intermediate. However, there is little systematic study on this topic, with the exception of the analytical work by Clavin and Joulin (1997), although the conditions there may not be directly relevant for turbulent flows. We

attempt to address this problem by following/tracking specific points on the flame surface, by displacing them with the vector sum of their local flame speeds in the surface normal direction and local flow velocities. The stretch time history that a flame particle carries can be directly used to answer fundamental questions of broader practical relevance like turbulent flame speed, flame extinction, etc. It is noted that since we only have velocity and flame surface information in a 2D plane, we can only track the motion of a surface point that is constrained to remain on the 2D plane. Adopting the definition and notation of Pope (1988) for surface points, the motion of such in-plane flame particle can be described by:

$$\frac{d}{dt}\mathbf{X}_{2D}^{F}(t) = \mathbf{U}_{2D}\left(\mathbf{X}_{2D}^{F}[t],t\right) + S_d\left(\mathbf{X}_{2D}^{F}[t],t\right)\mathbf{n}_{2D}^{F}\left(\mathbf{X}_{2D}^{F}[t],t\right). \tag{3.3}$$

Here $\mathbf{X}_{2D}^{F}$ is the position vector of the flame particle on the flame edge at time *t*. The local displacement flame speed could be modeled as $S_d = S_L - \delta_M \mathbf{K}$, with δ_M obtained from laminar expanding flame experiments. Figures 3.3a and 3.3b show the time evolution of the flame edges colored with local tangential strain rates K_t and stretch rate due to pure curvature K_c respectively for CH_4-air 1 atm 2000 rpm flame condition. The path tracked by a representative flame particle is shown by black circles. On the first frame the flame particles are positioned on each of the flame edge points and are allowed to evolve according to Eqn. (3.3). Since the edge is located only at discrete points on the grid, it might happen that the flame particles do not land up exactly on the edge at the subsequent instant. In that case the edge point, which is at the shortest distance from the new flame particle position, is considered to be the updated position. The K_s and K_c time histories from each flame particle are subsequently auto-correlated. The integral of the ensemble averaged autocorrelation function yields the integral time scale for K_t and K_c. These time scales are averaged over all the runs over the same conditions to yield the final persistence time scales τ_{P,K_t} and τ_{P,K_c} of K_t and K_c respectively. For example:

$$\tau_{P,K_c} = \left\langle \int_0^{\infty} \overline{K_c\left(\mathbf{X}_{2D}^{F}[t],t\right) K_c\left(\mathbf{X}_{2D}^{F}[t+\tau],t+\tau\right)} d\tau \right\rangle, \tag{3.4}$$

where the bar and angular brackets denote time and ensemble average respectively. These are shown in Fig. 3.3c for all experimental conditions. We find that for all conditions under study τ_{P,K_t} remains rather invariant within a range of 400-600 μs. However, the τ_{P,K_c} shows a much higher degree of sensitivity in response to the change in u_{rms}, pressure and hence Re_T, and varies from about $\tau_{P,K_c} \sim 800\mu s$ for the CH_4, 1 atm, 4000 rpm case to about $\tau_{P,K_c} \sim 1.8ms$ for the C_4H_{10}, 5 atm, 2000rpm case. In general considering all cases under study, the τ_{P,K_c} is greater than τ_{P,K_t} by nearly a factor of 2. This suggests that strain rate due to pure curvature might be a more persistent quantity than that due to tangential strain in the current configuration and conditions. Even without flame particle tracking, from Figs. 3.3a and b we qualitatively observe that the

geometry of the flame edges remains correlated with the evolution in time for both cases. Local curvature being a measure of the local geometry thus quantitatively emerges as a rather persistent quantity for the flames under consideration. Though these persistence time scales are obtained from 2D flame particle tracking, it is to be recognized that experimentally tracking the motion in 3D is extremely challenging if not currently impossible, given the necessity of simultaneous volumetric imaging of flow and reactive isosurfaces with high time resolution. Hence the representative persistence time scale information of tangential strain rate and curvature gleaned from the 2D motion of the surrogate flame particle remains to be of substantial interest.

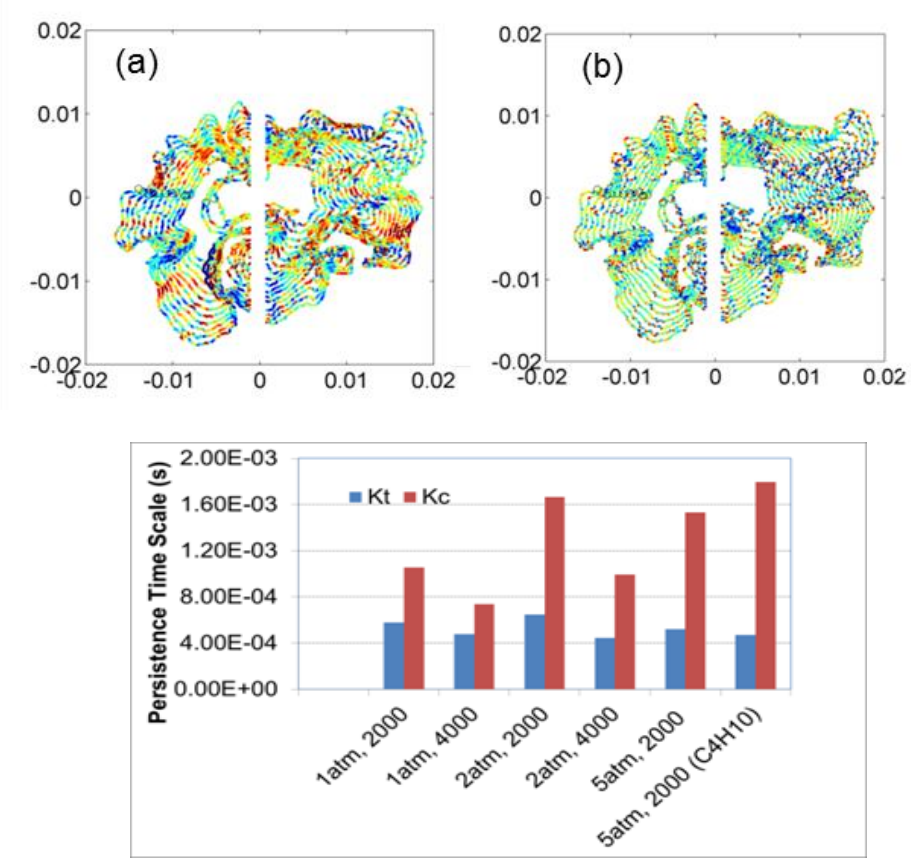

Fig. 3.3 *: Evolution of flame edge with time, coloured by (a) K_t (b) K_c for CH_4-air Φ=0.9, 2000rpm, p=1atm; (c) Persistence time scales of K_c and K_t over all experimental conditions. CH_4-air was used in the first five cases*

4. Effect of Turbulence on Ignition Kernel:

Ignition of a combustible mixture by a stimulus kernel is of relevance to many terrestrial and extraterrestrial phenomena and applications, such as the various modes of engine operation [Reitz (2013)], prevention of accidental explosions [Kissel et al (1973)], and initiation of the supernova explosion [Woosley et al (2011)]. Frequently, such ignition occurs in flows that are highly turbulent, involving a wide range of time and length scales. Previous studies have

advocated that turbulence renders ignition more difficult [Ballal (1977), Kaminiski et al (2000), Bradley et al (2004), Ahmed et al (2006), Shy et al (2010)], based on the notion that turbulence increases the dissipation rate of the deposited kernel energy before an embryonic flame either has the time or is aerodynamically favorable to develop.

Such an argument, however, does not take into consideration the evolution and dynamics of the structure of the nascent flame kernel after it is formed. To appreciate these influences, and to facilitate exposition of the rationale of the experimental investigation to be presented later, it is first noted that the burning rate and consequently the extinction propensity of a laminar flame segment of surface area A, subjected to generalized aerodynamic stretching which accounts for the collective effects of flow nonuniformity, flame curvature and flame unsteadiness, is characterized by the stretch rate $K = d(\ln A)/dt$ [Law (2006)]. Analysis in the limit of large activation energy E_a for an assumed one-step overall reaction typically yields a relation [Ronney and Shivashinsky (1989), Sun and Law (2000), Law (2006)] having the functional form:

$$s^2 \ln s^2 = -\alpha\kappa \tag{4.1}$$

where s is the local, stretched flame speed scaled by the steady unstretched flame speed, κ is the stretch rate K scaled by the laminar flame time, and α is commonly referred to as the Markstein number, which indicates the sensitivity of the flame responses, such as the propagation speed, to stretch. Various theoretical expressions for α have been derived [Pelce and Clavin (1982), Betchold and Matalon (2001), Matalon and Matkaowsky (1982), Clavin and Graña-Otero (2011)], accounting for effects of diffusive transport and thermal expansion, the temperature dependence of the transport properties, mixture composition, general reaction orders, and recently a modeled two-step kinetic scheme. These results show that, depending on the definition of the flame location and specification of the chemical kinetics, the specific form for α can be different for flame curvature and flow straining. The dominant influence, however, is the extent that the mixture's effective Lewis number (Le) deviates from unity, as quantified by the parameter (Le - 1), where Le is defined as the ratio of its thermal diffusivity to the controlling mass diffusivity. This is demonstrated for example by the expression [Matalon et al (2003)],

$$\alpha = \frac{\sigma}{(\sigma-1)}\int_1^\sigma \frac{\lambda(x)}{x}dx + \frac{Ze(Le-1)}{2(\sigma-1)}\int_1^\sigma \frac{\lambda(x)}{x}\ln\left(\frac{\sigma-1}{x-1}\right)dx \tag{4.2}$$

where σ is the thermal expansion ratio across the flame, $\lambda(x)$ the normalized thermal conductivity as a function of the normalized temperature x, $Ze = E_a(T_b - T_u)/RT_b^2$ the Zel'dovich number, R the universal gas constant, and T_b and T_u the burned and unburned gas temperatures, respectively.

Two observations can be made from the above theoretical results. First, by examining the linearized form of Eq. 4.1, $s \approx 1 - \alpha\kappa$, it is apparent that the trend of the flame response is qualitatively affected by the sign of a combined, diffusivity-affected stretch term, $\Lambda = (Le - 1)\kappa$,

weakened for $\mathit{\Lambda} > 0$, and strengthened otherwise. Second, as a consequence of the nonlinear feedback between transport and chemical heat release [Sun and Law (2000)], Eq. 4.1 exhibits a dual-solution response for $\mathit{\Lambda} > 0$, indicating the potential of extinction at the associated turning point.

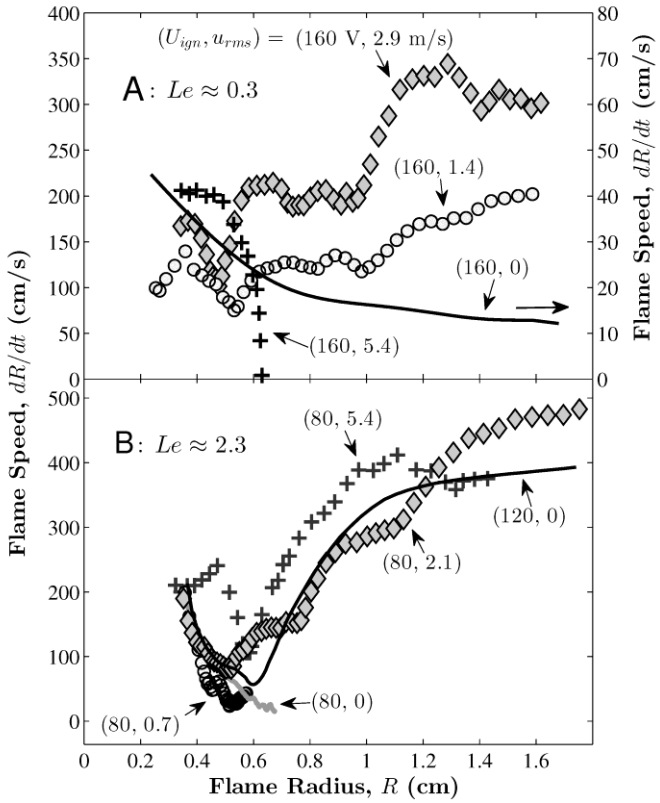

*Fig. 4.1: Flame speed versus flame radius for (**A**) lean H_2/air at $\phi = 0.18$, and (**B**) rich H_2/air at $\phi = 5.1$, at different ignition voltages and turbulent levels. The flame radius in turbulent cases is defined as $R = \sqrt{\overline{A}/\pi}$, where $\overline{A}$ is the area enclosed by the flame edge tracked from the Schlieren image. The spark gap distance d_g is 0.30 mm for **A** and 0.58 mm for **B***

Applying the above concept to the sustenance of a spark-ignited, *continuously-expanding* spherical flame in quiescence, it is first recognized that since the stretch rate is given by $K = 2d(\ln R)/dt > 0$, the flame burning rate is governed by the sign of (Le - 1). It is then obvious that, if enough ignition energy is supplied to establish a flame kernel, then a $Le < 1$ flame would be strengthened by stretch and thus continuously propagate, albeit with progressively reduced velocity, until it reaches the adiabatic planar flame limit as $R \rightarrow \infty$. However, for a $Le > 1$ flame, since the burning rate is weakened by stretch, even it can be initially established, the ignition energy may not be sufficient to sustain flame propagation when all this energy is dissipated before R has reached a critical flame radius, R_c, leading to extinction. Thus if the ignition energy is slightly larger than that barely sufficient to sustain flame propagation at R_c, then the

propagation velocity will exhibit a minimum at R_c, and increase thereafter to attain the adiabatic planar flame limit as $R \rightarrow \infty$. Consequently, we expect the flame speed to be small at the state of R_c. Indeed, unsteady analyses and simulations of the initiation of the spherical flame [Frankel and Shivashinsky (1984)] have shown that R_c corresponds well to the Zel'dovich's flame ball radius, R_Z, with a vanishing propagation flame speed [Zel'dovich et al (1985)].

The above distinctively different behaviors are respectively shown in Figs. 4.1A and 4.1B, for the instantaneous propagation velocity $dR(t)/dt$, for lean and rich H_2/air mixtures whose *Le*'s are respectively < 1 and > 1; the experimental specifications are given later when presenting the results in turbulence. It is seen from the solid lines that, for the quiescent situation of no turbulence, $u_{rms} = 0$, an *Le* (= 0.3) < 1 flame will continuously propagate, with monotonically decreasing velocity, as long as sufficient ignition energy, varied by the spark discharge voltage U_{ign}, is supplied. However, an *Le* (= 2.3) > 1 flame will extinguish if the ignition energy is not sufficient (U_{ign} = 80 V), but with sufficient ignition energy (U_{ign} = 120 V) will continuously propagate after having attained a minimum, critical radius.

Let us now consider ignition in turbulence, and for the sake of clarity focus on the critical state at which the ignition energy is just barely sufficient to initiate an expanding, *Le* > 1 flame in quiescence. It is clear that, in the presence of turbulence, the otherwise spherical flame with a uniform, positive, curvature will be wrinkled, leading to an embryonic flame structure with both locally positive and negative curvatures. Furthermore, local flows with extensive and compressive strain rates, with $K > 0$ and < 0, can also be induced. The net effect is that the flame surface will be locally subjected to additional $\Lambda > 0$ and < 0 stretch effects. The key point to note here is that since the flame in quiescence is already at the incipient state of extinction over its entire surface, any flame segments that are subjected to additional $\Lambda > 0$ effect in turbulence are still susceptible to extinction. However, the burning intensity of the flame segments that are subjected to $\Lambda < 0$ effect will be increased, moving them away from incipient extinction and consequently can collectively serve as local ignition sources to sustain the global flame structure.

With the above expository anticipation, the present work then aims to explore such a possibility, which may alter the traditional view on the criteria of ignition in turbulent flows, and as such highlight the necessity to incorporate the dynamics of the embryonic flamelet structure into the description and prediction of ignition.

We undertook a well-controlled experimental approach to categorically study the effects of turbulence on an ignition kernel. Tests were conducted in the constant-pressure, optically accessible, vessel, detailed in the section of experimental details. The ignition system was similar to those used in automotive engines, with a slight modification by replacing the spark plug by two tungsten wires of 250-μm diameter and centered axially. The spark is generated by discharging a 33 μF capacitor through an ignition coil with a 134:1 turn-ratio. Voltage (U_{ign}) across the capacitor was made variable from 50 V to 170 V, allowing the ignition energy to vary.

In designing the matrix of the experimental investigation, it was noted that previous works on the interaction of turbulence and ignition kernel were limited to inhibited ignition, ostensibly due to the small deviations in *Le* from unity. Therefore we extended the experiments to cover a wide range of *Le*, especially focusing on mixtures with *Le* sufficiently greater than unity such that ignition could be limited by the extent of stretch that the flame kernel experiences. At the same time we also considered mixtures with $Le \approx 1$ or $Le < 1$ to provide a complete description of the phenomena. We selected H_2/O_2 mixtures for most of the investigation because it allows flexible variation of *Le* due to the drastic difference between the molecular weights of hydrogen and oxygen. This can be achieved by varying the H_2/O_2 ratio, namely the equivalence ratio ϕ of the mixture (defined to be the fuel/oxygen ratio relative to the stoichiometric mixture), thereby changing the diffusivity of the deficient, hence controlling, reactant. Furthermore, since the H_2/O_2 oxidative chemistry is relatively simple and also reasonably well established, the present data can be usefully adopted in further computational studies on issues of turbulence-chemistry interaction in general and of this practically relevant problem in particular.

We first demonstrate the possible enhancement of ignition by turbulence through direct, time-resolved Schlieren images, using a fuel rich H_2/air mixture of $\phi = 5.1$, which has a large *Le* of 2.3 since the controlling, deficient reactant is O_2, while the thermal diffusivity is controlled by that of H_2. Figs. 4.2A and 4.2B respectively show a successful and a failed ignition event in quiescence ($u_{rms} = 0$), with an ignition voltage, $U_{ign} = 120$ V and a smaller value of 80 V. This result therefore agrees with the earlier discussion on the dependence of ignition on the energy input. The measured velocities of these images, together with those for the lean mixture of $\phi = 0.18$, with $Le = 0.3$, are those shown in Figs. 4.1B and 4.1A, respectively.

If we next maintain the ignition voltage constant at 80 V but progressively increase the turbulence level, Figs. 2B-E show that the structure of the flame kernel is changed from a positively stretched spherical surface to a multitude of wrinkled flamelets of both positive and negative curvatures, and that ignition is achieved at $u_{rms} = 2.9$ m/s. This result therefore supports the notion that for $Le > 1$, a combustible mixture can be ignited in turbulence with an ignition energy that is not enough to ignite the same mixture in quiescence.

We have extensively mapped out the ignition boundary for the $\phi = 5.1$ mixture in terms of the turbulence intensity and the ignition energy, summarized in Fig. 3A. It is found that the minimum discharge voltage required for successful ignition in the presence of moderate turbulence ($u_{rms} = 2.9$ m/s) is 65 V (indicated by blue circles filled with green color in figure), which is substantially reduced from the voltage required for ignition in quiescence (100 V). Based on the relation $E_{ign} = CU_{ign}^2$, where E_{ign} and C are the discharge energy and capacitance, respectively, this result implies that the minimum ignition energy can be lowered by a few factors with the presence of turbulence.

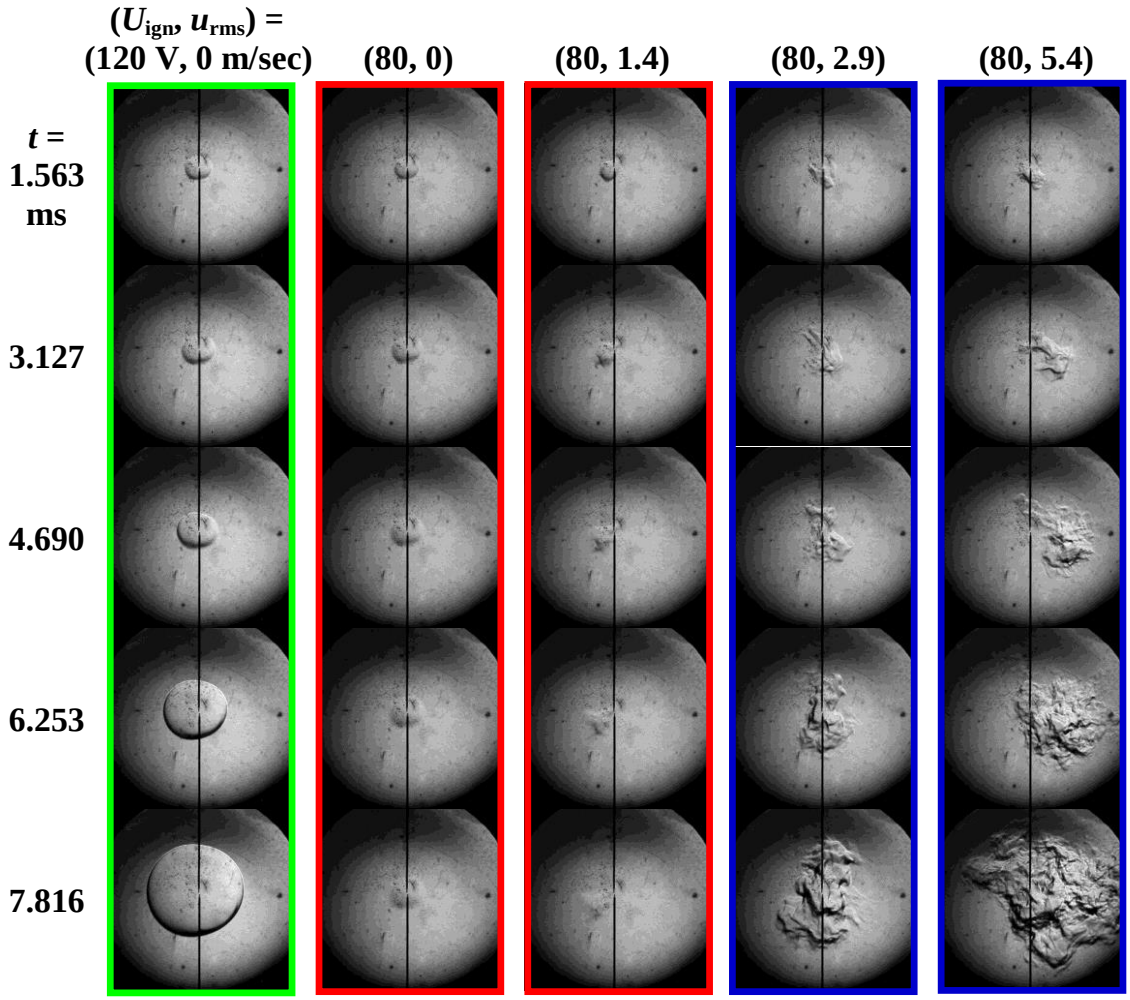

Fig. 4.2*: Sequential Schlieren images of flame kernel development for H_2/air at ϕ = 5.1 (Le ≈ 2.3), at different ignition voltages and turbulent levels. Schlieren imaging signal is proportional to the density gradient of the flow field, a good indicator of the flame front. The view for each image is 65 mm × 65 mm. t is time after discharge.*

Having demonstrated the facilitating effect of turbulence on the *Le* > 1, rich H_2/air mixtures, it is necessary to investigate the response of lean mixtures, whose *Le* is less than unity because the controlling, deficient reactant is now H_2 and the thermal diffusivity is dominated by those of O_2 and N_2. As anticipated earlier, since a flame kernel with *Le* < 1 is always facilitated by positive stretch in quiescence, ignition is expected to be successful as long as a flame kernel can be established. Turbulence, in this case, increases the dissipation rate of the deposited kernel energy and as such renders ignition progressively more difficult with increasing turbulence intensity, eventually leading to extinction. Our results on lean H_2/air mixtures (ϕ = 0.12 - 0.2, Figs. 3B and 3C) confirm this mechanistic interpretation and are also consistent with the conclusions of previous studies which, as noted earlier, were mostly based on *Le* ≈ 1 mixtures.

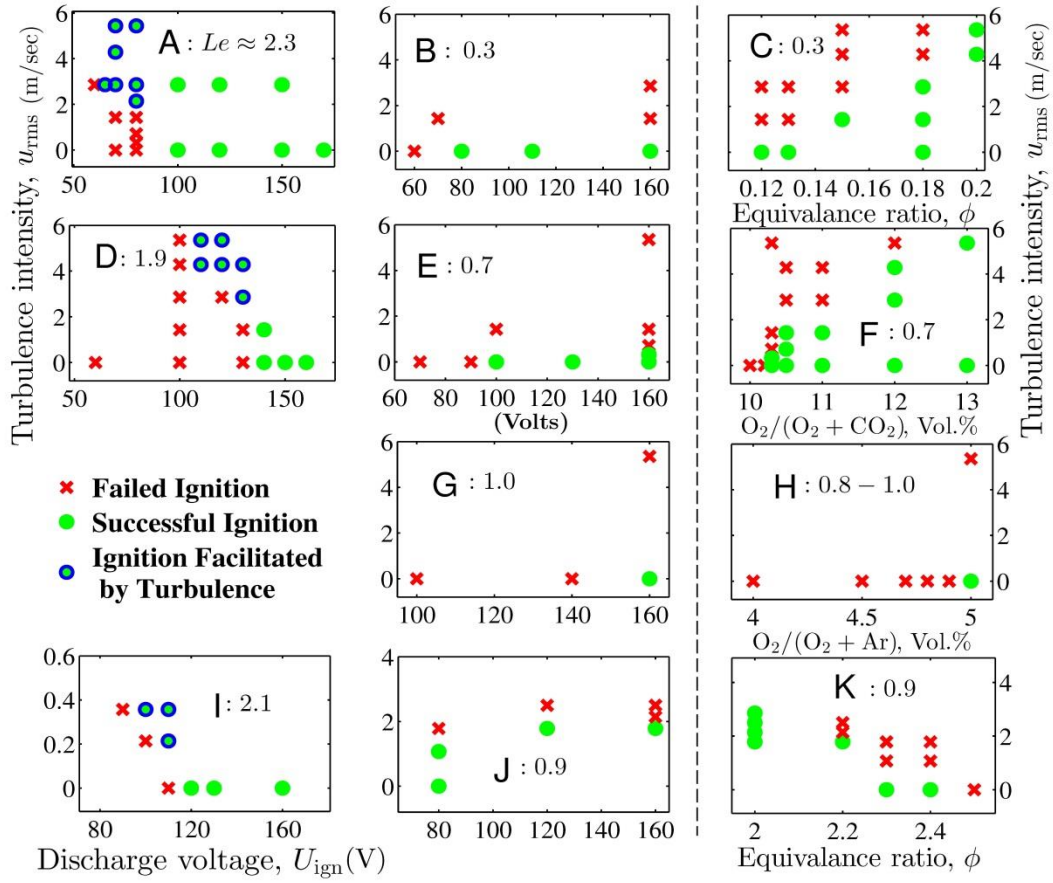

Fig. 4.3*: Ignition test results plotted against turbulence intensity (u_{rms}) and discharge voltage (U_{ign}) or mixture reactivity, represented by the H_2/O_2 ratio or the amount of inert gas.* ***(A)*** *H_2/air at equivalence ratio (ϕ) = 5.1* ***(B)*** *H_2/air at ϕ = 0.12* ***(C)*** *H_2/air for fixed U_{ign} = 160 V.* ***(D)*** *H_2/O_2/He at ϕ = 1.0, $O_2/(O_2$+He) Vol.% = 8.0%* ***(E)*** *$H_2/O_2/CO_2$ at ϕ = 1.0, $O_2/(O_2$+ CO_2) Vol.% = 10.3%* ***(F)*** *$H_2/O_2/CO_2$ at ϕ = 1.0 for fixed U_{ign} = 160 V* ***(G)*** *H_2/O_2/Ar at ϕ = 1.0, $O_2/(O_2$+ Ar) Vol.% = 5.0%* ***(H)*** *H_2/O_2/Ar at ϕ = 1.0 for fixed U_{ign} = 160 V.* ***(I)*** *n-C_4H_{10}/air at ϕ = 0.7* ***(J)*** *n-C_4H_{10}/air at ϕ = 2.2* ***(K)*** *n-C_4H_{10}/air for fixed U_{ign} = 160 V. Initial pressure and temperature for all tests are 1 atm and 298 K. The Le shown in figure is defined to be the effective Lewis number of a combustion mixture, based on theory in [24]. The spark gap distance d_g is 0.58 mm for case* ***A****, 0.30 mm for cases* ***B-H****, and 0.80 mm for cases* ***I-K****. Here we identify three stages.* ***Failed Ignition*** *(red crosses): where ignition kernel fails to grow to a propagating flame, either due to lack of ignition energy in quiescent environment or faster dissipation by turbulence.* ***Successful Ignition*** *(green dots): where ignition kernel containing sufficient energy grows to a flame with or without the presence of turbulence.* ***Ignition Facilitated by Turbulence*** *(blue open circles filled with green color): where ignition kernel grows to a flame in the presence of turbulence, but fails to do so in quiescence if supplied with the same ignition energy.*

We also need to rule out the possibility that the controlling ignition chemistry could be different for fuel rich and fuel lean mixtures, causing the observed phenomena. To remove such a possibility, we manipulated the values of *Le* by changing the inert bath gas from N_2 to (He, Ar,

CO_2), with the fuel/oxygen ratio fixed such that the controlling lean-vs.-rich chemistry is not affected. It is seen (Figs. 3D-H) that the facilitating effect of turbulence is again manifested only for $Le > 1$ mixtures, and that the effect can be flipped from inhibiting to facilitating solely by changing the inert bath gas while ϕ is fixed at unity. In particular, turbulence facilitates ignition with He, a light inert which substantially increases the thermal conductivity and thus *Le*; while with heavier inerts such as CO_2 and Ar, *Le* becomes less than or near unity and as a result ignition is inhibited. These extensive sets of experiments therefore rule out the possibility that the distinct turbulence effects for fuel lean and fuel rich conditions are due to different chemical kinetics.

Finally, in order to provide even further substantiation of the phenomena and concept advanced herein, and for fuels other than H_2, we have flipped the lean-vs.-rich aspect of the mixture by using *n*-butane (*n*-C_4H_{10}) as the fuel, whose *Le* are greater and smaller than unity for lean and rich mixtures because of the substantially larger molecular weight of *n*-butane relative to that of oxygen. Thus *lean* (*rich*) *n*-butane/air mixtures should exhibit behavior similar to those of *rich* (*lean*) H_2/air mixtures, respectively.

Figs. 4.3I-K summarizes the ignition test results for a lean and a rich *n*-butane/air mixture, whose *Le*'s are 2.1 and 0.9 respectively. It is seen that ignition is indeed facilitated for the $Le > 1$, lean mixture. The above extensive results therefore demonstrate that ignition enhancement by turbulence for mixtures with large *Le* is of a general nature, irrespective of fuel, equivalence ratio and inert.

The above result unambiguously shows the role of *Le* in propagation of an embryonic ignition kernel in a turbulent environment. More categorically, it shows that for $Le > 1$ conditions, turbulence enhances the growth of the kernel in presence of turbulence as opposed to that in the case of $Le < 1$, where turbulent mixing or dissipation simply blows away the kernel before it develops into a flame. This immediate raises a question that if dissipation is not important at all for the $Le > 1$ conditions. To answer the question we studied such conditions of $Le > 1$, primarily with lean *n*-butane (*n*-C_4H_{10}) mixtures, with increasing turbulent intensities. We found for the ignition voltage/energy where turbulence assisted ignition is possible, i.e., even though the ignition fails at the laminar condition with certain level of turbulence the kernel grows into a flame, there exists an upper boundary of turbulence intensity, beyond which turbulent suppresses ignition. These results and the complete map for lean *n*-butane (*n*-C_4H_{10}) are shown in Fig. 4.4, which shows the non-monotonic response of the ignition kernel with the turbulence intensities. This is caused by the increased dissipation with the higher turbulence intensity, which overcomes the benefits of locally negative stretched flamelets whose strong propagation for $Le > 1$ mixtures caused the turbulence assisted ignition possible for lower levels of turbulence intensity.

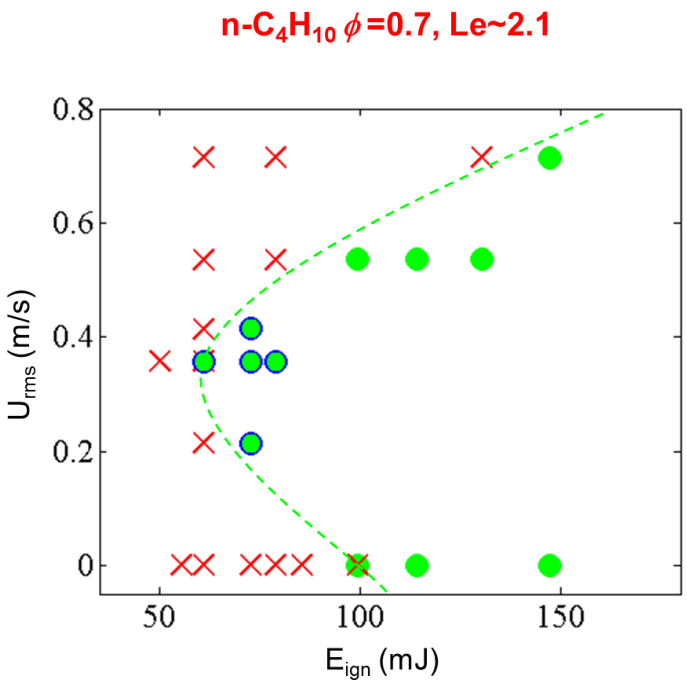

Fig. 4.4*: Ignition map for n-C_4H_{10}/air at ϕ = 0.7. Here we identify the ignition window with the presence of three stages.* ***Failed Ignition*** *(red crosses): where ignition kernel fails to grow to a propagating flame, either due to lack of ignition energy in quiescent environment or faster dissipation by turbulence.* ***Successful Ignition*** *(green dots): where ignition kernel containing sufficient energy grows to a flame with or without the presence of turbulence.* ***Ignition Facilitated by Turbulence*** *(blue open circles filled with green color): where ignition kernel grows to a flame in the presence of turbulence, but fails to do so in quiescence if supplied with the same ignition*

In summary, while turbulence is usually believed to suppress ignition due to the enhanced dissipation of localized ignition energy, we have experimentally demonstrated that it can actually facilitate ignition under conditions in which ignition is limited by the difficulty of the flame kernel to transition into an expanding flame. This is possible through an embryonic flamelet structure consisting of segments subjected to both positive and negative stretch, while quiescent ignition generates only positive stretch through the positive curvature over the entire expanding, smooth flame surface. Such an understanding is of both practical and scientific significance. For example, explosion tests in quiescence may underestimate the risk of accident; while engine flows can also be optimized to reduce misfire for ultra-lean, clean, fuel-efficient operations, recognizing that engine fuels are large hydrocarbons such that their lean burning corresponds to *Le* > 1 situations. Furthermore, while studies of the supernova explosion have always assumed the initial existence of a flame that subsequently transitions to a detonation wave, perhaps it would be of interest to also investigate situations for which the establishment and sustenance of such a flame may not be possible in the first place, recognizing the fact that the *Le* for supernovae is exceedingly large [Glazyrin *et al*], of the order of 10^4.

References:

Ahmed S & Mastorakos E (2006), Combustion and Flame 146, 215

Ahmed SF, Balachandran R & Mastorakos E (2007), Proceedings of the Combustion Institute, 31, 1507

Ballal DR & Lefebvre AH (1977), Proceedings of the Royal Society A. 357, 163.

Bechtold JK & Matalon M, Combustion and Flame (2001), 127, 1906

Bradley D, Sheppard CGW, Suardjaja IM & Woolley R (2004), Combustion and Flame 138, 55

Chaudhuri S, Akkerman V & Law CK (2011), Physical Review E, 84, 026322

Chaudhuri S, Wu F, Zhu DL & Law CK (2012), Physical Review Letters, 108, (2012), 044503

Chung SH & Law CK (1984), Combustion and Flame 55, 183

Clavin P & Joulin G (1997), Combustion Theory and Modelling, 1 (4), 429

Clavin P & Graña-Otero JC (2011) Journal of Fluid Mechanics, 686, 187

Creta F & Matalon M (2011), Journal of Fluid Mechanics, 680, 225

Damköhler G. (1940), Zeitschr. f. Elektrochemie, 46, 601

Frankel ML & Sivashinsky GI (1984), Combustion Science and Technology, 40, 257

Glazyrin SI, Blinnikov SI & Dolgov A (2013), MNRAS, 433, 2840

Kaminski CF, Hult J, Alden M, Lindenmaier S, Dreizler A, Mass U & Baum M (2000), Proceedings of the Combustion Institute, 28, 399

Kelley AP & Law CK (2009), Combustion and Flame, 156 (6), 1844

Kerstein A, Ashurst W & Williams FA (1988), Physical Review A, 37, 2728-2731

Kissell FN, Nagel AE & Zabetaki MG (1973), Science 179, 891

Law CK (2006), Combustion Physics (Cambridge University Press)

Markstein GH (1951), Journal of Aeronautical Sciences 18, 199.

Matalon M & Matkowsky BJ (1982), Journal of Fluid Mechanics 124, 239

Matalon M, Cui C & Bechtold JK (2003), J. Fluid Mech. 487, 179

Pelce P &. Clavin P (1982), Journal of Fluid Mechanics 124, 219.

Pope SB (1988), International Journal of Engineering Sciences 26 (5), 445

Reitz RD (2013), Combustion and Flame 160, 1

Shy SS, Liu CC & Shih WT (2010) Combustion and Flame 157, 341

Tse S, Zhu D L & Law CK (2004), Review of Scientific Instruments, 75, 1, 233

Woosley SE, Kerstein AR & Aspden AJ (2011), Astrophysical Journal. 734, 37

Zel'dovich YB, Barenblatt GI, Librovich VB & Makhyiladze GM (1985), The Mathematical Theory of Combustion and Explosions, (Springer)

Archival Publications during Reporting Period

1. "Flame surface statistics of constant-pressure turbulent expanding premixed flames," by Abhishek Saha, Swetaprovo Chaudhuri and Chung K. Law, Physics of Fluids, Vol. 26, 045109 (2014); DOI: 10.1063/1.4871021.
2. "Facilitated ignition in turbulence though differential diffusion," by Fujia Wu, Abhishek Saha, Swetaprovo Chaudhuri and Chung K. Law, Physical Review Letters, Vol. 113, 024503 (2014); DOI: 10.1103/PhysRevLett.113.024503
3. "On flame-turbulence interaction in constant-pressure expanding flames," by S. Chaudhuri, A. Saha and C. K. Law, Proceedings of the Combustion Institute, Vol 35 (2), 1331-1339 (2015);. DOI: 10.1016/j.proci.2014.07.038

Changes in research objectives (if any): NA

Additional Information: NA

Change in AFOSR Program Manager, if any:

Extensions granted or milestones slipped, if any: NA

1.

1. Report Type

Final Report

Primary Contact E-mail

Contact email if there is a problem with the report.

cklaw@princeton.edu

Primary Contact Phone Number

Contact phone number if there is a problem with the report

+1-609-258-5271

Organization / Institution name

Princeton University

Grant/Contract Title

The full title of the funded effort.

PHYSICAL AND CHEMICAL PROCESSES IN TURBULENT FLAMES

Grant/Contract Number

AFOSR assigned control number. It must begin with "FA9550" or "F49620" or "FA2386".

FA9550-13-1-0119

Principal Investigator Name

The full name of the principal investigator on the grant or contract.

Prof. Chung K Law

Program Manager

The AFOSR Program Manager currently assigned to the award

Dr. Chiping Li

Reporting Period Start Date

03/15/2013

Reporting Period End Date

03/14/2015

Abstract

The two-year subject program, conducted through tight coupling between experiment, theory and computation, and reported in high impact journal articles, has focused on the dynamics of turbulent flames mainly for hydrocarbon fuels in environments simulating various operational aspects of aero-engines. The thrust for this program constitutes of three major areas of turbulent combustion: (1) Flame surface statistics, (2) Flame-turbulence interaction, and (3) Effects of turbulence on the growth of ignition kernel.

Using high-speed Mie-scattering we investigated the local flame surface statistics of constant-pressure turbulent expanding flames. First, the statistics of the local length ratio is experimentally determined from high-speed planar Mie scattering images of spherically expanding flames, with the length ratio on the measurement plane, at predefined equiangular sectors, defined as the ratio of the actual flame length to the length of a circular-arc of radius equal to the average flame radius. Assuming isotropic distribution of such flame segments we then convolute suitable forms of the length-ratio probability distribution functions (pdfs) to arrive at the corresponding area-ratio pdfs. It is found that both the length ratio and area ratio pdfs are near log-normally distributed and shows self-similar behavior with increasing radius.

To quantify the effect of the flame on the turbulence the mean and the rms of the flow field are measured over a range of conditions both in the presence and absence of the flame using High Speed PIV. The distributions of stretch rate contributions from different terms such as tangential straining, normal straining

and curvature are also obtained. It is found that the normal straining displays non-Gaussian pdf tails whereas the tangential straining shows near Gaussian behavior. We have further tracked the motion of the edge points that reside and co-move with the edge of the flame kernel during its evolution in time, and found that within the measurement conditions, on average the persistence time scales of stretch due to pure curvature exceed those due to tangential straining by at least a factor of two.

Finally we experimentally demonstrated that contrary to the belief that ignition of a combustible mixture by a high-energy kernel is more difficult in turbulence than in quiescence because of the increased dissipation rate of the deposited energy, it can actually be facilitated by turbulence for mixtures whose thermal diffusivity sufficiently exceeds its mass diffusivity. In such cases, turbulence breaks the otherwise single spherical flame of positive curvature, and hence positive aerodynamics stretch, into a multitude of wrinkled flamelets possessing either positive or negative stretch, such that the intensified burning of the latter constitutes local sources to facilitate ignition.

Distribution Statement

This is block 12 on the SF298 form.

Distribution A - Approved for Public Release

Explanation for Distribution Statement

If this is not approved for public release, please provide a short explanation. E.g., contains proprietary information.

SF298 Form

Please attach your SF298 form. A blank SF298 can be found here. Please do not password protect or secure the PDF The maximum file size for an SF298 is 50MB.

AFD-070820-035.pdf

Upload the Report Document. File must be a PDF. Please do not password protect or secure the PDF . The maximum file size for the Report Document is 50MB.

Report_AFOSR_2015_CKLAW_PU.pdf

Upload a Report Document, if any. The maximum file size for the Report Document is 50MB.

Archival Publications (published) during reporting period:

1. “Flame surface statistics of constant-pressure turbulent expanding premixed flames,” by Abhishek Saha, Swetaprovo Chaudhuri and Chung K. Law, Physics of Fluids, Vol. 26, 045109 (2014); DOI: 10.1063/1.4871021.
2. “Facilitated ignition in turbulence though differential diffusion,” by Fujia Wu, Abhishek Saha, Swetaprovo Chaudhuri and Chung K. Law, Physical Review Letters, Vol. 113, 024503 (2014); DOI: 10.1103/PhysRevLett.113.024503
3. “On flame-turbulence interaction in constant-pressure expanding flames,” by S. Chaudhuri, A. Saha and C. K. Law, Proceedings of the Combustion Institute, Vol 35 (2), 1331-1339 (2015);. DOI: 10.1016/j.proci.2014.07.038

Changes in research objectives (if any):

NA

Change in AFOSR Program Manager, if any:

NA

Extensions granted or milestones slipped, if any:

NA

AFOSR LRIR Number

LRIR Title

Reporting Period

Laboratory Task Manager

Program Officer

Research Objectives

Technical Summary

Funding Summary by Cost Category (by FY, $K)

	Starting FY	FY+1	FY+2
Salary			
Equipment/Facilities			
Supplies			
Total			

Report Document

Report Document - Text Analysis

Report Document - Text Analysis

Appendix Documents

2. Thank You

E-mail user

Jun 11, 2015 11:58:47 Success: Email Sent to: cklaw@princeton.edu